Journal of Colloid and Interface Science 529 (2018) 224–233

Contents lists available at ScienceDirect

Journal of Colloid and Interface Science

journal homepage: www.elsevier.com/locate/jcis

Controllable internal mixing in coalescing droplets induced by the solutal Marangoni convection of surfactants with distinct headgroup architectures

Jerome J. Nash [a], Patrick T. Spicer [b], Kendra A. Erk [a,*]

[a] School of Materials Engineering, Purdue University, West Lafayette, IN 47907, USA
[b] School of Chemical Engineering, The University of New South Wales, Sydney 2052, Australia

GRAPHICAL ABSTRACT

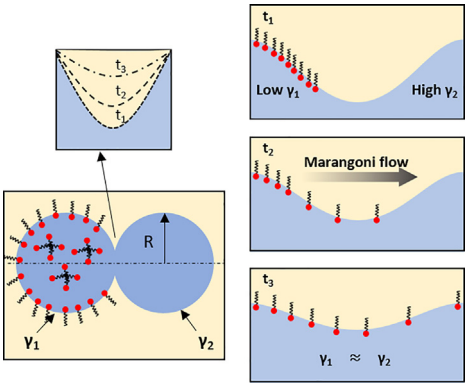

ARTICLE INFO

Article history:
Received 12 March 2018
Revised 4 June 2018
Accepted 5 June 2018
Available online 6 June 2018

Keywords:
Marangoni flow
Convection
Mixing
Coalescence

ABSTRACT

Through several complementary experiments, an investigation of the bulk and interfacial flows that emerged during the coalescence of two water-in-oil droplets with asymmetric compositional properties was performed. By adding surfactant to one of the coalescing droplets and leaving the other surfactant-free, a strong interfacial tension gradient (i.e., solutal Marangoni) driving energy between the merging droplets generated pronounced internal mixing. The contributions of two distinct types of surfactant, anionic ammonium lauryl sulfate (ALS) and cationic cetyltrimethylammonium bromide (CTAB) on the rate of coalescence bridge expansion and on the generation of opposing flows during coalescence were investigated. All coalescence experiments supported the power law relation between the radius of the expanding connective liquid bridge and time, $r_b \propto t^{1/2}$. However, the presence of surfactant decreased the magnitude of the prefactor in this relationship due to induced interfacial solutal Marangoni convection. Experiments showed that packing efficiency, diffusivity, and bulk concentration of the selected surfactant are vital in solutal Marangoni convection and thus the degree and timescale of internal mixing between merging droplets, which has yet to be adequately discussed within the literature. Denser interfacial packing efficiency and lower diffusivity of CTAB produced stronger opposing bulk and interfacial flow as well as greater bulk mixing. A discussion of how optimized surfactant selection and solutal Marangoni convection can be used for passively inducing convective mixing between coalescing drops in microfluidic channels when viscosity modulation is not feasible is provided.

* Corresponding author.
E-mail address: erk@purdue.edu (K.A. Erk).

https://doi.org/10.1016/j.jcis.2018.06.011
0021-9797/

1. Introduction

The coalescence of two identical droplets, and the corresponding bulk fluid flows that emerge, has been studied at length in the literature [1–5]. However, far less attention has been given to the coalescence of binary droplets with asymmetric physical properties, despite its importance to many industrial and research applications including enhanced oil recovery [6], emulsification [7], microfluidic reactors [8], and functional microparticle fabrication [9–11].

Many additional examples can be found in the literature of microfluidic applications that utilize the coalescence of droplets as a vital processing step in material fabrication. However, mixing immiscible phases in microfluidic devices often proves difficult because of the low Reynolds number flows encountered within microchannels. Several researchers have shown that the combination of immiscible fluids in microchannels can be improved with modified channel designs [12–14] or, quite often, by modulating the viscosity of one or both of the coalescing fluids to achieve desired bulk convective mixing [15,16]. While several detailed coalescence studies have investigated the effects of variable external oil phase viscosity on the generation of bulk flows in coalescing water droplets [17,18], little attention was given to the potential influence of polar surfactant headgroup architecture in the generation of the observed opposing interfacial and bulk flows. Moreover, altering the viscosities of the bulk fluids is not always a viable option in microfluidic applications (for example, when high throughput is a processing requirement, or when a system is restricted to fluids with predetermined viscosities). Thus, additional routes for inducing a similar degree of internal mixing under these restrictions are necessary, and currently, no experimental studies in the literature have sought to provide insight into how appropriate surfactant selection can influence this phenomenon.

Utilizing solutal Marangoni convection, also known as the Gibbs-Marangoni effect [19,20], provides a compelling avenue for inducing desired bulk flows in coalescing droplet systems, without the need for modulating bulk fluid viscosity. The Gibbs-Marangoni effect can be induced simply by adding a dilute concentration of a highly surface-active solute to one of the fluid droplets, while keeping the second drop initially free of any surfactant, then bringing the droplets into contact. When the two fluid droplets coalesce, a highly curved connective liquid bridge forms between them and expands rapidly due to interfacial stresses. In the inertial regime, a scaling relation derived from a simple physical argument can be used to describe the expansion of the coalescence bridge [4]. This scaling law predicts linear proportionality between the radius of the connective liquid bridge, r_b ($=D_b/2$), and the square root of the coalescence time, $t^{1/2}$, given by the equation, $D_b/2 \propto (R\gamma/\rho_{out})^{1/4}t^{1/2}$, where R is the initial drop radius, γ is the interfacial tension, and ρ_{out} is the density of the outer fluid.

As bridge expansion proceeds, the resulting fluid motion acts to pull the droplets together to form a single, larger drop. However, in the presence of an induced surface tension (i.e., surfactant concentration) gradient between the droplets, opposing interfacial and bulk flows can emerge. This is because surfactant molecules become nonuniformly distributed at the interface along the highly curved, connective liquid bridge separating the surfactant-laden and surfactant-free drops [21]. Relaxation to a homogenous surfactant coverage does not proceed primarily by diffusion, but by a far more rapid process (i.e., the Gibbs-Marangoni effect) where the surfactant molecules at the interface swiftly migrate toward regions of highest local interfacial tension. This in turn generates interfacial motion in the direction of the surfactant concentration gradient that acts tangentially to the merging droplets, which is accompanied by bulk motion in the adjacent fluid layers. Consequently, bulk flows which drive the droplets together under the influence of a favorable reduction in capillary pressure, $\Delta P = 2\gamma/R$, become unbalanced with interfacial flows. This ultimately results in opposing interfacial and bulk convective motion and can lead to pronounced bulk fluid mixing.

It has been shown that the mobility [22], as well as the degree of equilibrium interfacial adsorption of low molecular weight surfactants [23,24], can vary substantially depending on the nature of the surfactant's polar headgroup in a polar solvent such as water (i.e., whether it is anionic, cationic, nonionic, or zwitterionic). These interfacial characteristics are also well-known to have demonstrated importance in the occurrence of film rupture and coalescence for surfactant-laden fluid interfaces [25,26]. Therefore, it would stand to reason that strategically modulating the interfacial mobility, equilibrium saturation adsorption, and adsorption-desorption kinetics of the added surfactant would enable interested parties to control coalescence related phenomena, such as passively-induced internal mixing between emulsion droplets in the presence of a surfactant concentration gradient. Optimized design of such small-scale processes will require the ability to identify appropriate surfactants based on their physicochemical properties and performance in applications like diagnostic chips and microreactor systems. Thus, this work seeks to demonstrate several key mechanisms relating the adsorption of two oppositely charged ionic surfactants and the manifested solutal Marangoni flows that drive bulk mixing between coalescing aqueous droplets in a viscous surrounding oil. Generalized relationships between the interfacial properties of low molecular weight surfactant and their potential influence on bulk coalescing phenomena are also provided.

Many detailed experimental and theoretical analyses have been performed which elucidate early-stage coalescence phenomena of uniform liquid droplets both in air and an external liquid [1–5]. However, fully developed mixing behaviors in the later stages of coalescence (i.e., several milliseconds following the onset of coalescence) are often a primary concern in microfluidic reactor applications [8,27]. Therefore, to aid in the design of such systems, the specific aims of this work were to (1) investigate the late-stage coalescence behavior of binary liquid droplets with an induced surfactant concentration gradient along the connective liquid bridge, and (2) illustrate how controlling equilibrium adsorption and solutal Marangoni motion through appropriate surfactant selection can encourage varying degrees of bulk fluid mixing. Through several complementary experiments, including equilibrium surfactant adsorption measurements, high-speed image processing, and concentration gradient-induced interfacial velocity measurements via particle tracking, we provide new insights into the fundamental relationships between optimized surfactant selection and bulk fluid mixing. Considering that the adsorption and interfacial spreading behavior of surfactants can vary dramatically depending on the electrostatic interactions of the surfactant present at the fluid interface in the bulk aqueous solution [28], detailed investigations which further elucidate the role of surfactant selection in the development of varying degrees of opposing flows within coalescing binary droplets are essential.

2. Materials and experimental methods

2.1. Materials

The external liquid phase used during drop coalescence measurements was a triglyceride oil (Stepan Company, CAS # 73398-61-5) with a manufacturer reported viscosity of 25 mPa·s and density of 0.95 g cm^{-3}, both at 25 °C. The oil was double-filtered through a chromatography column containing alumina (Fisher,

CAS # 1344-28-1) to remove trace surface-active impurities prior to use. The droplets consisted of aqueous solutions prepared with water passed through a Filmtec™ reverse osmosis membrane (total dissolved solids $\leq$ 15 ppm, Dow Chemical Company). The two commercially available surfactants used in this study, ammonium lauryl sulfate, ALS (anionic surfactant, 30% in water, CAS # 2235-54-3) and cetyltrimethylammonium bromide, CTAB (cationic surfactant, $\geq$99%, CAS # 57-09-0), were obtained from Sigma-Aldrich and used without further purification. The blue dye added to the surfactant-free droplet in each binary droplet coalescence measurement as an aid for visualizing bulk motion was purchased from Queen Fine Foods Pty Ltd. The flat metal capillaries (18-gauge $\times$ 1.0″ blunt tip dispensing needles) used in droplet coalescence experiments were obtained from CML Supply.

2.2. Visualizing rapid binary drop coalescence

A schematic of the experimental setup used for visualizing binary liquid droplet coalescence is shown in Fig. 1. Experiments were performed using a pair of three-axis micromanipulators (Sensapex) secured to z-axis translational stages (THORLABS) flanking an inverted optical microscope (AE31, Motic Microscopes). Two water droplets with asymmetric compositional properties, each having an initial diameter of 2 mm (unless otherwise specified) were formed at the tips of 18-gauge metal capillaries and were made to contact at negligible approach velocities ($\sim$0.01 mm s^{-1}) in a clear petri dish containing the low viscosity triglyceride oil (5 mL working volume). Coalescence of the binary droplets was captured with a high-speed camera (Phantom v7.3) at 11,000 frames per second. Measurements of the bridge expansion kinetics were performed via image processing using open-source ImageJ software [29].

A concentration gradient along the connective liquid between the two merging water drops was generated by adding the surfactant of interest to the leftmost coalescing droplet (Fig. 1), while keeping the rightmost droplet surfactant-free. The surfactant-loaded droplet in each experiment contained either ALS or CTAB at a concentration of 2.5×10^{-3} mol L^{-1}, which was near the experimentally determined critical micelle concentration (CMC) for each surfactant type. The relevant data used in determining the CMC for each surfactant is provided in Section 2.3. This initial bulk surfactant concentration was chosen because near and above the CMC, the chemical potential of the surfactant negligibly changes and as a result conditions at the interface do not change [30]. Thus, the surfactant-laden droplet interface in this experimental setup represents an interfacial monolayer near saturation equilibrium. At the chosen bulk concentration, the equilibrium interfacial tension of the oil-water interface was 3.40 ± 0.48 mN m^{-1} for ALS and 3.01 ± 0.41 mN m^{-1} for CTAB, as determined by the drop shape analysis technique (Section 2.3).

To help visualize the emergent bulk fluid motion during droplet coalescence, dye was added to the surfactant-free droplet at a concentration of 0.1 g L^{-1}. The addition of dye did not substantially affect the oil-water interfacial tension (surfactant-free, pure droplet: γ = 23.67 ± 0.13 mN m^{-1}; surfactant-free, dyed droplet: γ = 21.42 ± 0.27 mN m^{-1}), and thus its contribution to the emergent coalescence flows was presumed to be negligible in comparison to the presence of the highly surface-active molecules, ALS and CTAB.

2.3. Determination of interfacial adsorptive properties at the oil-water interface

Interpreting the relationship between the induced bulk flows and the contributing interfacial Marangoni stresses of coalescing binary droplets requires knowledge of the equilibrated interfacial adsorption for each surfactant-laden droplet prior to merging. The effective interfacial tension values for pure and surfactant-laden oil-water interfaces were obtained using axisymmetric drop shape analysis with a contact angle goniometer/tensiometer (Ramé-Hart) following experimental procedures established in previous work by Nash and Erk [31]. The theory underpinning this technique and its corresponding application to study the effective interfacial tensions for air-liquid and liquid-liquid monolayers have been previously discussed in the literature [32,33]. In brief, the interfacial tension of each oil-water interface was determined by fitting the shape profile of an aqueous pendant drop suspended from the tip of a flat 12-gauge PTFE capillary immersed in oil to the theoretical profile prescribed by the Young-Laplace equation, $\Delta P = \gamma\left(\frac{1}{R_1} + \frac{1}{R_2}\right)$. This force balance relates the differential in pressure, ΔP, across a curved interface to its principle radii of curvature R_1 and R_2, and interfacial tension, γ. As surface active solutes become adsorbed to the interface, there is a demonstrable reduction in the capillary pressure. For a known pressure and interfacial curvature, the effective interfacial tension of the surfactant-laden interface can be directly measured.

The equilibrium interfacial adsorption isotherms for dilute aqueous solutions of ALS or CTAB in contact with triglyceride oil are provided in Fig. 2. In each adsorption experiment, the interfacial tension was measured over time for at least 45 min, or until a constant interfacial tension value was reached. The critical

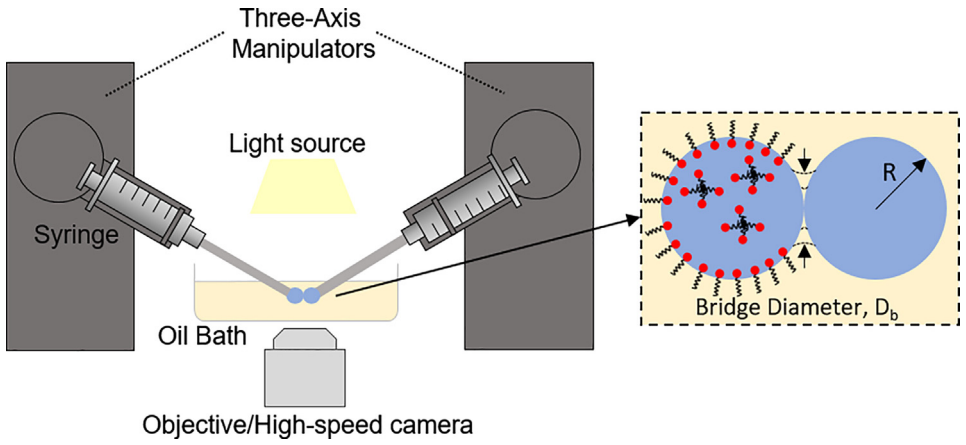

Fig. 1. An illustration of the experimental setup used to study coalescence phenomena between binary aqueous droplets in a surrounding oil. The leftmost aqueous droplet was laden with surfactant and the rightmost droplet was surfactant-free, yet contained a small concentration of dye to aid in flow visualization.

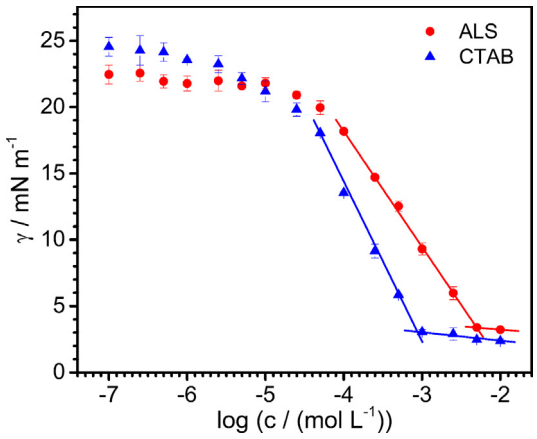

Fig. 2. Interfacial tension, γ, versus log of surfactant concentration, c, in aqueous solution at 23 °C for the triglyceride oil-water interface measured by the drop shape analysis technique. Lines represent best-fitting straight lines of the data in the low and high surfactant concentration regimes for each surfactant. The slope value of the best-fitting line in the low surfactant concentration regime was used in the determination of the surface excess concentration, Γ_m, for ALS and CTAB.

micelle concentration (CMC's) for each surfactant was determined graphically from Fig. 2 as the intersection of the linear fits to the low and high concentration regimes for each surfactant. Experimental CMC values for ALS and CTAB at 23 °C were ca. 5.5×10^{-3} mol L^{-1} and 0.95×10^{-3} mol L^{-1}, respectively. The CMC value obtained here for ALS closely corresponded to the value found in the literature, 6.25×10^{-3} mol L^{-1} [34]. Likewise, the CMC value obtained here for CTAB agreed well with previous observations in the literature of 0.9×10^{-3} mol L^{-1} [35] and 1×10^{-3} mol L^{-1} [36].

The surface excess concentration, Γ_m, corresponds to the maximum concentration of surfactant adsorbed to the oil-water interface of the surfactant-laden droplet at equilibrium and was approximated for each surfactant using the Gibbs adsorption equation, $\Gamma_m = -\frac{1}{mRT}\left(\frac{d\gamma}{d\log c}\right)_{T,P}$, where γ is the interfacial tension (mN m^{-1}), c is the bulk surfactant concentration (mol L^{-1}), R is the gas constant, T is the temperature (K), and the integer, m, accounts for the charge interactions within the polar head group of the surfactant. For dilute aqueous solutions containing a single, 1:1 ionic surfactant in the absence of excess salt, m = 4.606, which was taken for both anionic ALS and cationic CTAB [37,38]. Substituting the slope value of the best-fitting straight line in the low surfactant concentration regime from the interfacial tension versus log of surfactant concentration curve for $\frac{d\gamma}{d\log c}$ in the Gibbs adsorption equation, Γ_m was calculated for ALS and CTAB at the triglyceride oil-water interface. The minimum molecular area, A_{min} ($Å^2$ $molecule^{-1}$), was then determined from the equation, $A_{min} = \frac{1\times10^{20}}{\Gamma_m N_A}$, where N_A is Avogadro's number. (Table 1).

Table 1
Surface excess concentrations and minimum molecular areas calculated for ALS and CTAB at 23 °C at the triglyceride oil-water interface.

Surfactant	Surface excess concentration, $\Gamma_m/(10^{-6}$ mol $m^{-2})$	Minimum molecular area, A_{min}/ ($Å^2$ $molecule^{-1}$)
Ammonium Lauryl Sulfate (ALS)	0.76	218
Cetyltrimethylammonium bromide (CTAB)	1.07	156

2.4. Determination of surfactant-induced interfacial spreading velocity, U_s

The experimental setup used to study the interfacial spreading velocity, U_s, of each surfactant when introduced into the pure triacylglyceride oil-water interface is shown in Fig. 3. The displacement of tracer particles (hollow glass spheres, 9–13 μm diameter, Sigma-Aldrich, CAS # 65997-17-3) seeded at the pure oil-water interface initiated by the introduction of a surfactant-loaded water droplet to the pure oil-water interface and driven by solutal Marangoni flow was measured.

The motion of tracer particles was measured at a planar oil-water interface because this experimental scheme specifically enabled the measurement of Marangoni-induced flow rates under the effect of a surfactant concentration gradient at the oil-water interface. Ensuring that the measured flow rates were obtained for tracer particles located specifically at the oil-water interface and not within one of the subphases was most directly accomplished with a droplet coalescing with a planar oil-water interface.

Preparation of a planar triglyceride oil-water interface containing the seeded glass spheres was performed using a modified optical microscopy cell and methodology adapted from the work of Park et al. [39]. The cell used here consisted of a polystyrene petri dish (height 1 cm, outer diameter of 40 mm) and a concentric polystyrene cylinder (height 1 cm, outer diameters of 30 mm). An aluminum ring was inserted into the bottom of the inner polystyrene cylinder to pin the contact line of the oil-water interface. The inner cylinder was secured to the polystyrene petri dish using a fast curing epoxy and 0.1 mm glass spacers. This allowed for the oil-water system to achieve hydrostatic equilibrium, ensuring that a planar oil-water interface could be attained via the addition or removal of water from the outer portion of the sample cell.

After forming a planar oil-water interface free of any solutes, an oil droplet containing tracer particles was directly added to the upper oil phase of the sample cell. This yielded a seeded tracer concentration of $\sim 4 \times 10^6$ particles-cm^{-2} at the interface, a concentration which was necessary for accurate particle tracking measurements and quantifying the interfacial spreading velocities resulting from the introduction of surfactant. It should be noted that at this concentration, seeded tracer particles displayed slight aggregation. Very large aggregates would be expected to display lower interfacial spreading velocities in comparison to unaggregated primary particles due to their larger mass and could therefore introduce some degree of uncertainty into the measured interfacial spreading velocities in this experimental setup. However, the largest aggregates observed in this study consisted of 2–3 primary particles, and measurements of the steady-state, fully developed displacement rates for these aggregates were indistinguishable from the measured displacement rates of unaggregated, interfacially adsorbed primary particles.

Following the seeding of tracer particles, the experimental cell was stabilized for 15 min, then a 10 μL droplet of either surfactant solution was formed at the tip of a metal capillary within the oil layer. The droplet was equilibrated for an additional 30 min within the upper oil layer prior to contact with the planar oil-water interface to allow for saturated interfacial adsorption of the surfactant. Finally, the droplet was lowered slowly (~0.01 mm s^{-1}) to contact the planar oil-water interface and the resulting isotropic tracer particle motion was captured using an inverted microscope and high-speed camera (Photron Mini UX) at 2000 frames per second. Due to the remarkably high energy of attachment for micrometer-scale particles at the oil-water interface [40], particle motion was presumed to be approximately two-dimensional for the duration of particle spreading. Care was taken to quantify the displacement of at least five tracer particles from two separate

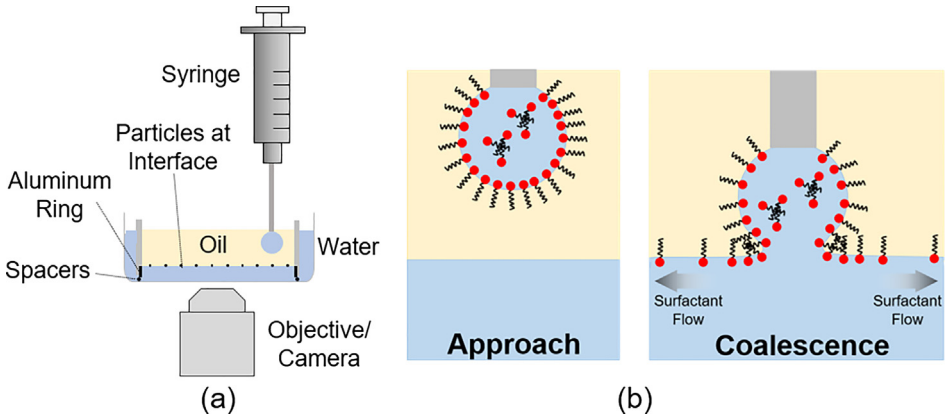

Fig. 3. Schematic representation of the experimental setup used to quantify interfacial spreading velocities, U_s, under an induced interfacial tension gradient at the triglyceride oil-water interface. A side view depicting the introduction of a surfactant loaded water droplet at the surfactant-free, oil-water interface (containing tracer particles) is shown in (a) and an illustration of the surfactant diffusion mechanism, quantified by measuring the rate of displacement for tracer particles attached to the interface, is shown in (b).

experiments for each oil-water-surfactant system, measured manually using ImageJ software.

3. Results and discussion

3.1. Effect of surfactant type on bridge expansion and bulk mixing during the coalescence of equally sized drops

Our investigation of surfactant contributions in the generation of opposing flows within coalescing binary droplets begins with the consideration of two surfactant-free droplets sharing an equivalent initial diameter, 2R (=2 mm), and approximately equal oil-water interfacial tensions (surfactant-free, undyed droplet: γ_1 = 23.67 ± 0.13 mN m^{-1}; surfactant-free, dyed droplet: γ_2 = 21.42 ± 0.27 mN m^{-1}). Analysis of bridge expansion for the two, equally sized coalescing droplets with no added surfactant revealed that this system closely obeyed the $D_b/2 \propto (R\gamma/\rho_{out})^{1/4}t^{1/2}$ scaling relation over the entire duration of droplet merging (Fig. 4), agreeing well with the experimental observations of previous researchers [17,18].

For equally sized coalescing droplets, where one of the drops contained 2.5 × 10^{-3} mol L^{-1} ALS, the $D_b/2 \propto t^{1/2}$ scaling relation was also closely obeyed, but a slightly reduced slope in the experimental data was observed. This indicates that the value of the prefactor, $(R\gamma/\rho_{out})^{1/4}$, in the coalescence scaling relation was influenced by the presence of ALS. Likewise, an even more pronounced decrease in the slope of this scaling relationship became apparent at longer times for systems containing 2.5 × 10^{-3} mol L^{-1} CTAB. This further suggests that the gradient in interfacial tension and timescale of solutal Marangoni flow of the chosen surfactant along the interface of expanding liquid bridge has a demonstrable influence on the value of the prefactor in the scaling relation, which was not explicitly accounted for or discussed in its derivation.

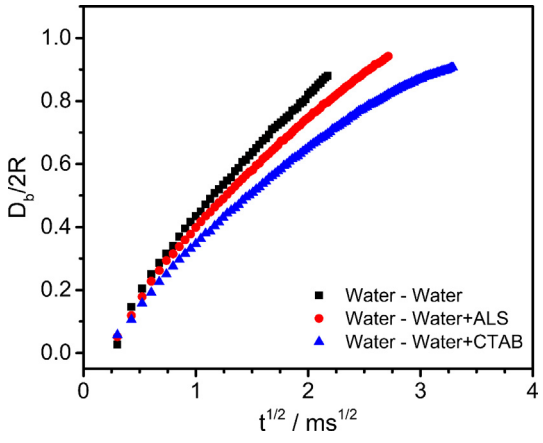

Fig. 4. Kinetics of expansion for the connective bridge separating spherical droplets with an equivalent initial diameter, 2R (=2 mm). The data represent the increase in the connective bridge diameter, D_b, relative to 2R, as a function of the square-root-of-time, $t^{1/2}$, succeeding the onset of droplet coalescence.

The characteristic time scale for coalescence of two equally sized drops with equal interfacial tensions in inviscid flow is set by $\tau_C = \sqrt{(\rho R^3)/\gamma}$ [41]. For the merging of two 0.75-mm radius water drops in the inertial regime, with γ = 23 mN m^{-1}, τ_C is ~ 4.2 ms. This characteristic relaxation time closely approximates the experimentally measured time required for the expanding bridge between the surfactant-free water droplets to become equal to the initial drop diameter for the system shown in Fig. 5a. This approximation is less representative in the presence of a surfactant concentration gradient, which can be seen from the data in Fig. 5b and 5c, for ALS and CTAB, respectively. Each of these systems require a longer duration for the diameter of the expanding bridge to be equal to the initial diameter of the drops. The observed increase in τ_C for systems containing ALS or CTAB, as well as the clear difference between their corresponding τ_C values, suggests that interfacial adsorptive and convective properties of the surfactant contribute to the decrease in the value of the prefactor in the coalescence scaling relation. This observation is discussed in greater detail in Section 3.3.

Fig. 5a illustrates that negligible internal mixing occurred during the merging of surfactant-free droplets due to the generation of two balanced, plug-flow water jets which converged at the propagating coalescence neck. In this instance, the interfacial tensions of the converging droplets are balanced and thus no tangential stress was competing with the bulk fluid motion of the merging drops. This behavior agreed well with experimental observations of previous researchers [17,18]. Contrarily, coalescence of binary droplets with non-uniform compositions of a surface-active species displayed pronounced internal convective mixing during the coalescence process, the degrees of which strongly depended on the surfactant present at the oil-water interface of the surfactant-laden droplet.

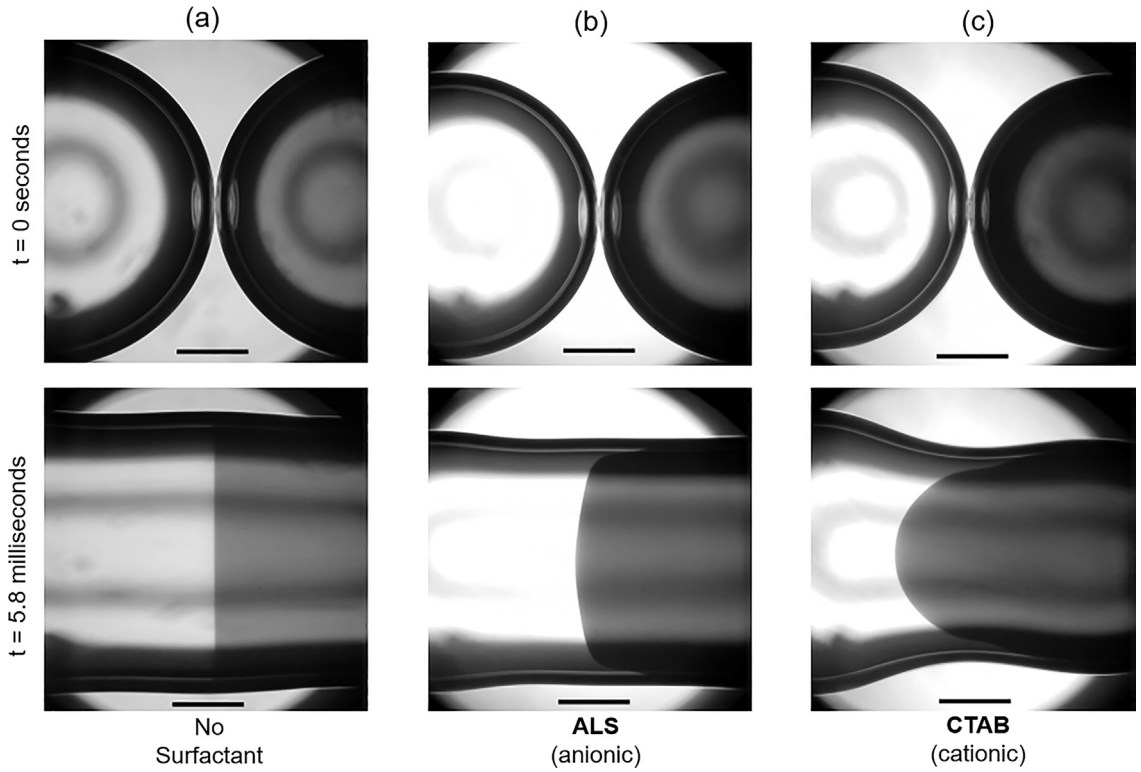

Fig. 5. Temporal shape profiles of equally sized water droplets coalescing in triglyceride oil. The leftmost droplet in each image contained either (a) no surfactant, (b) 2.5×10^{-3} mol L^{-1} ALS, or (c) 2.5×10^{-3} mol L^{-1} CTAB, while the rightmost droplet in each image was surfactant-free, with dye added for flow visualization. The absence or presence of opposing flows at the interface and within the bulk of the merging droplets illustrate the effect of interfacially adsorbed surfactant molecules. Differences in the curvature of the jetted fluid following coalescence in (b) and (c) demonstrate the influence of surfactant headgroup architecture on the relative magnitude of these induced flows. The scale bars in each image are 0.5 mm in length.

Distinct bulk fluid motion was observed in the presence of either anionic ALS or cationic surfactant CTAB for equally sized droplet with a capillary pressure ratio of $\Delta P_2/\Delta P_1 \approx 5$ (where ΔP_1 and ΔP_2 are the capillary pressures of the leftmost droplet and the rightmost droplet, respectively) and are shown in Fig. 5b and 5c. The presence of surfactant in the undyed, leftmost drop led to the formation of a fluid jet which propagated from the bulk of dyed, surfactant-free drop as direct result of this droplet's higher capillary pressure. For the binary droplets system containing 2.5×10^{-3} mol L^{-1} ALS, the motion of the jetted fluid appeared to occur under near plug flow conditions, with some discernable curvature of the jetting dyed fluid at later times. However, the internal mixing for the binary systems containing 2.5×10^{-3} mol L^{-1} CTAB was demonstrably more pronounced, displaying a much higher curvature of the jetted fluid at later stages of coalescence (i.e., after 5.8 ms).

3.2. Influence of surfactant type on the development of bulk fluid jetting

To further aid in illustrating the marked influence of surfactant in the jetting behavior observed for binary droplet systems, the initial diameters of the two merging droplets were modulated by increasing the initial diameter of the leftmost droplet to 2.2 mm and decreasing the initial diameter of the rightmost droplet to 1.0 mm. Fig. 6a shows that for asymmetrically sized droplets, both free of any added surfactant and of approximately equal interfacial tension, droplet merging led to only slight jetting of the fluid within the smaller diameter, surfactant-free droplet into the larger droplet as a direct result of the relatively small capillary pressure gradient ($\Delta P_2/\Delta P_1 \approx 2$) originating from the difference in initial droplet sizes. However, the magnitude of the capillary pressure gradient was insufficient to induce a great deal of internal mixing.

In the case of binary droplet systems that contained a concentration gradient of either ALS or CTAB, the difference in diameter and interfacial tension between the binary droplets provided a much larger capillary pressure ratio ($\Delta P_2/\Delta P_1 \approx 11.5$) and thus a greater driving energy for jetting of the fluid from the smaller droplet into the larger droplet containing surfactant during coalescence. The late-stage flows that emerged under these experimental conditions are shown in Fig. 6b and 6c, respectively. For the binary droplet system with 2.5×10^{-3} mol L^{-1} ALS present in the surfactant-laden droplet, the profile of the fluid jetted from the smaller, surfactant-free droplet took the shape of a bulb-like plume with a relatively large diameter forming near the apex of the jetted fluid and slightly narrower base. Similarly, for the binary droplet system containing 2.5×10^{-3} mol L^{-1} CTAB, the late-stage internal flow also resulted in the formation of a fluid jet with a large bulb and narrow base. However, the jetting that occurred in this case was demonstrably stronger, with the formation of a mushroom-shaped plume of dyed water and a far narrower base.

The difference in the shape of the jetted fluid that emerged in systems containing ALS or CTAB stemmed from the magnitudes of the convective mixing generated by the opposing bulk and Marangoni interfacial flows upon droplet coalescence. As the fluid from the dyed droplet flowed through the propagating coalescence neck, an interfacial diffusional flux developed in the opposite direction, as interfacially adsorbed surfactant molecules in the surfactant-laden droplet migrated from regions of high concentration to low concentration. This in turn generated eddy currents within the

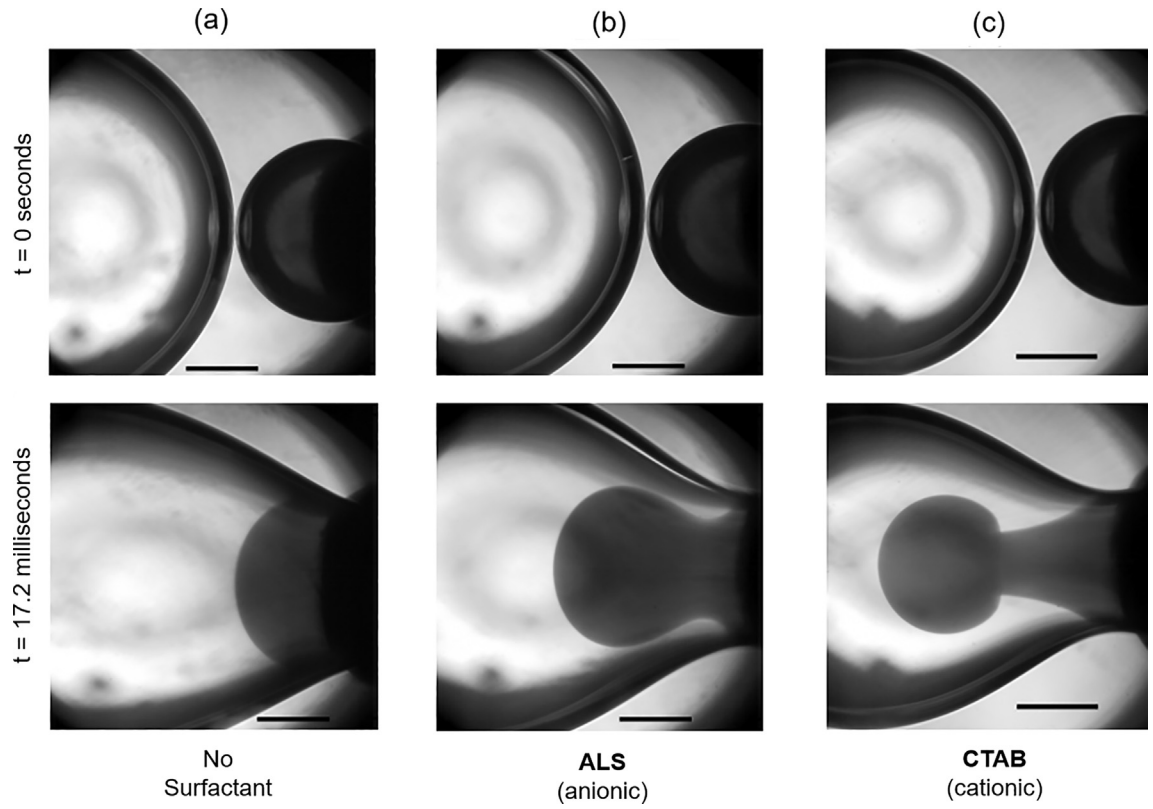

Fig. 6. Flow profiles depicting the formation of fluid jets of different sizes for asymmetrically sized water droplets coalescing in triglyceride oil. The leftmost droplet in each image contained either (a) no surfactant, (b) 2.5×10^{-3} mol L^{-1} ALS, or (c) 2.5×10^{-3} mol L^{-1} CTAB, while the rightmost droplet in each image was surfactant-free, with dye added for flow visualization. The scale bars in each image are 0.5 mm in length.

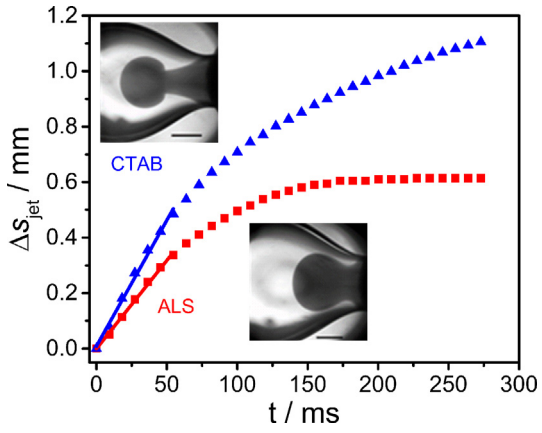

Fig. 7. Displacement of the jetted fluid apex, Δs_{jet}, originating from the surfactant-free droplet into the surfactant-laden droplet as a function of time, t, succeeding droplet contact for asymmetrically sized droplet systems. Micrograph insets depict the position of the fluid jets 17.2 ms after the onset of coalescence. The scale bars in each image are 0.5 mm in length.

bulk of the merging droplets, just beneath the interface. In the case of CTAB, the driving energy for interfacial flux appeared to be sustained for a longer time than in the case of ALS, which led to more pronounced eddy currents and thus the observed jetting behavior.

Furthermore, assessment of the displacement of the jetted fluid apex as a function of time for asymmetrically sized binary droplet systems, containing either ALS or CTAB (Fig. 7), indicates a clear difference in the induced fluid motion. The rate of fluid jetting during the initial stages of coalescence was roughly 30% faster for the droplet system containing cationic CTAB compared to the analogous system containing anionic ALS (9.08 mm s^{-1} and 6.37 mm s^{-1}, respectively, from a linear regression fit to the initial data in Fig. 7). In the following sections, we discuss in detail our experimental basis for attributing differences in the emerged jetting phenomena to differences in the magnitudes of the induced interfacial Marangoni flows accompanying each surfactant. The jetting phenomena observed between merging drops with an induced surfactant concentration gradient can also be explained by the induction of Marangoni convection, where low interfacial tension liquid along the oil-water interface of the coalescing neck is carried toward the higher interfacial tension regions in the surfactant-free droplet and accumulates. A localized increase in the hydrostatic pressure of this region follows and the development of a bulk flow of liquid from the surfactant-free droplet in the opposite direction of the Marangoni flow.

3.3. Comparison of adsorptive properties of ALS and CTAB at the triglyceride oil-water interface

Values for the surface excess concentration, Γ_m, in Table 1 indicate that CTAB molecules pack more densely at the triglyceride oil-water interface than ALS molecules, which is in line with previous experimental observations for the same or similar ionic surfactants at the oil-water interface [42,43]. The negatively charged moiety of 1:1 anionic surfactants leads these molecules to have a relatively large hydrodynamic diameter in comparison to cationic surfactants, which have a comparably small hydrodynamic diameter surrounding their positively charged headgroups [44]. These differences in the hydrodynamic volume surrounding the hydrophilic portions of each surfactant molecule lead to differences in their corresponding equilibrium adsorptive capabilities at immiscible fluid interfaces. As a direct result, anionic surfactants tend

to pack less efficiently at fluid interfaces than their cationic counterparts.

Each of the experimental observations of the differences in the magnitudes of solutal Marangoni convection for ALS and CTAB would also suggest that Γ_m has a pivotal role in the timescale of Marangoni interfacial flow. A more densely packed interfacial layer laden with surfactant would be expected to behave more rigidly in response to interfacial tension and surfactant concentration perturbations. This rigidity restricts lateral surface movements and solutal Marangoni convention. Thus, the timescale for solutal Marangoni flow would increase, as the interface overall would take longer to relax to a homogenous state (i.e., regions of high interfacial tension and regions of low interfacial tension would exist longer for more densely packed interfaces). Under these conditions, the high interfacial tension regions would apply a high tangential surface stress over a longer duration.

Likewise, considering that both ALS and CTAB are soluble in the aqueous phase, and can therefore adsorb and desorb from the bulk aqueous phase during droplet coalescence, both the surfactant's diffusion coefficient, *D*, and bulk surfactant concentration, c, would be expected to decrease the timescale of solutal Marangoni flow. A surfactant that can diffuse swiftly to the interface from the bulk would be expected to decrease the lifetime of interfacial tension gradient, (i.e., higher diffusion coefficients will favor a small concentration difference). Similarly, high concentrations of surfactant in the bulk would be expected to increase the overall adsorption rate of molecules near the interface, thus favoring small concentration gradients and reducing the timescale of solutal Marangoni convection.

The timescale of solutal Marangoni convection, τ_M, was approximated using these parameters in the equation, $\tau_M = \frac{\Gamma_m^2}{Dc^2}$. Incorporating the experimentally determined saturation adsorption values from Table 1, a bulk surfactant concentration of 2.5×10^{-3} mol L^{-1}, and diffusion coefficients of 5×10^{-10} m^2 s^{-1} for ALS [45], and 1×10^{-10} m^2 s^{-1} [46] for CTAB, the characteristic timescale of solutal Marangoni becomes ~0.2 ms for ALS and ~2 ms for CTAB. The order of magnitude difference in τ_M implies that the time required for interfacially adsorbed ALS molecules to respond and dampen interfacial tension fluctuation is far faster than that of CTAB molecules.

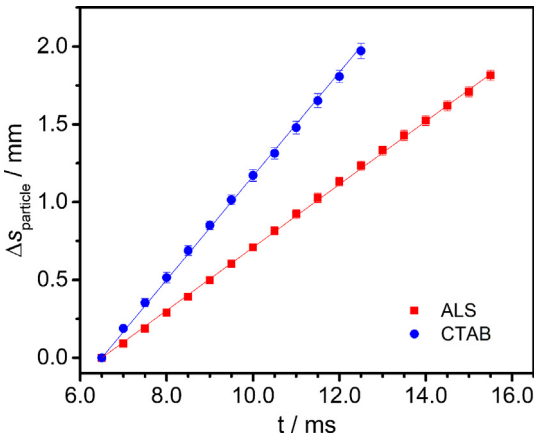

Fig. 8. Seeded tracer particle displacement, $\Delta s_{particle}$, versus time, t, following the introduction of a 2.5×10^{-3} mol L^{-1} aqueous droplet solution of anionic ALS or cationic CTAB surfactant at a planar triglyceride oil-water interface. Motion of the interfacially seeded tracer particles resulted directly from the induced surfactant concentration gradient of either ALS or CTAB. Data are shown for fully developed particle displacement rates, 6.5 ms after initial contact between the surfactant-laden drop and the planar oil water interface.

Regarding the flows observed in the coalescence of binary droplets with asymmetric compositions, the differences in interfacial motion between surfactants can be directly attributed to the magnitudes of the surfactant molecule's corresponding τ_M values. The timescale of solutal Marangoni convection is shorter than the characteristic coalescence timescale for two water droplets of equal diameters and interfacial tensions in the inertial regime for ALS (i.e., $\tau_M < \tau_C$). The driving energy for solutal Marangoni-driven convection is therefore relatively low because interfacial relaxation toward a homogenous interfacial tension along the coalescing bridge occurs faster than the time required for droplets to completely merge. In contrast, these timescales are very close in magnitude for systems containing CTAB (i.e., $\tau_M \approx \tau_C$). Thus, for CTAB molecules, relaxation toward homogenous interfacial tension takes much longer and is on the order of the time required for droplets to merge, which leads to the development of strong Marangoni-driven convection and competing bulk and interfacial flows.

3.4. Surfactant interfacial spreading properties under an induced concentration gradient

Fig. 8 shows the distance tracer particles travel as a function of time at the (initially) pure triglyceride oil-water interface following the introduction of a 2.5×10^{-3} mol L^{-1} aqueous droplet solution of either anionic ALS or cationic CTAB. These data represent the fully-developed motion of the particles, starting 6.5 ms after the introduction of surfactant into the pure oil-water interface.

These data show a clear difference in the steady-state spreading velocities, U_s, of seeded glass spheres under the induced concentration gradient (i.e. for ALS: $U_s = 0.202$ m s^{-1}; for CTAB, $U_s = 0.333$ m s^{-1}) which implies that the surface motion driven by unbalanced interfacial tensions in the presence of cationic CTAB molecules exceeds that of ALS molecules. Taking the initial droplet diameter, 2R (=2 mm), as the characteristic length scale, an estimation of the characteristic timescale for the oil-water interface to deform under the induced surfactant concentration gradient can be obtained from $\tau_D = 2R/U_s$. Approximations of τ_D yield 10 ms for ALS, and 6 ms for CTAB. These calculations for the characteristic timescales of interfacial deformation under and induced surfactant concentration gradient provide additional evidence that ALS molecules express a lower driving energy for solutal Marangoni-driven convection in comparison to CTAB molecules. As the driving energy for solutal Marangoni convection is lower for ALS, the overall motion of solutes attached to an oil-water interface when subjected to a concentration gradient would be expected to be influenced less by gradients in surfactant concentration because such gradients are short-lived.

The primary difference between the between measuring the interfacial spreading properties that develop in a droplet-planar coalescence system as opposed to a droplet-droplet system is the direction of the generated bulk flow between the aqueous droplet and planar water reservoir upon coalescence. In the case of the droplet-planar interface arrangement, the capillary pressure ratio, $\Delta P_2/\Delta P_1$ (where ΔP_1 and ΔP_2 are the capillary pressures for the surfactant-laden droplet and planar water reservoir, respectively), would approach zero because of the approximately infinite radius of curvature of the planar water reservoir. This would in turn produce a driving energy for bulk fluid motion to propagate from the surfactant-laden droplet into the surfactant-free, planar reservoir. This bulk fluid behavior stands in contrast to the bulk flows observed and quantified in Section 3, where bulk fluid motion was driven from the surfactant-free droplet into the surfactant-laden droplet due to the capillary pressure gradient. However, Marangoni-induced interfacial flows always act in the direction of the interfacial solute concentration gradient [19] and occur on a shorter timescale than bulk flows. Thus, the measured values

for the interfacial spreading velocities (i.e. the Marangoni-induced interfacial flow rates) would presumably be minimally influenced by the experimental arrangement.

It is worth noting once again that this difference in interfacial spreading was observed for two surfactants with distinct chemical architectures, which both reduced the interfacial tension of the pure triglyceride oil-water interface to approximately 3 mN m^{-1} at a high bulk concentration. The observed differences in interfacial spreading and jetting behavior during the coalescence of binary droplets with nonuniform compositional properties must be explained by additional interfacial relaxation mechanisms, which have not previously been studied in detail by the recent literature.

4. Summary and conclusion

Direct observation of the bulk flows generated during the coalescence of binary water-in-oil droplets with non-uniform physical properties and characterization of the contributive surfactant-induced interfacial phenomenon was performed. Mechanisms responsible for the observed opposing interfacial and bulk flows between merging surfactant-laden and surfactant-free droplets were also described. Fluid jets that developed during binary droplet coalescence were a direct result of convection driven solutal Marangoni flows which generated a rapid redistribution of low interfacial tension bulk fluid around the perimeter of the high interfacial tension bulk fluid. The degree of interfacial spreading and bulk fluid redistribution was greater for cationic CTAB molecules compared to ALS molecules due to stark differences in their equilibrium adsorption values, kinetic re-adsorptive rates during droplet coalescence, and overall tendency for expressing solutal Marangoni convection.

This work stands in contrast to work of previous researchers in that control over bulk flows during the coalescence of binary water droplets was induced entirely through optimized surfactant selection, with no need for modulation of the bulk viscosities of the outer or inner liquid phases. Our experimental results provide additional experimental confirmation that the governing power-law relationship for coalescing droplets in the inertial regime is obeyed in the presence of an induced surfactant concentration gradient, but the prefactor in this relationship is strongly dependent upon the interfacial properties of the added surfactant.

The analyses and relationships outlined in this work can be generalized for many different surfactant types, including anionic or cationic surfactants with longer alkyl chains than those investigated here, nonionic surfactants with various alkyl tail lengths, and zwitterionic surfactants. The parameters which are expected to shorten the timescale of solutal Marangoni-convection (while decreasing its driving energy) include the surfactant's diffusion coefficient and bulk concentration, while equilibrium interfacial saturation adsorption is the primary contributor in extending the timescale of solutal Marangoni convection. Thus, enhancing the bulk mixing of binary drops with an induced concentration gradient can be done by selecting a surfactant that packs densely at the immiscible fluid interface and adsorbs to the interface strongly. Zwitterionic and polymeric surfactant would likely be ideal candidates for such applications due to their relatively small diffusion coefficients and dense interfacial organization capabilities [47].

One of the most advantageous applications of using the controlled coalescence of droplets with asymmetric properties is in the synthesis of functional nanoparticles. Recently, Frenz et al. [27] demonstrated that magnetic iron oxide nanoparticles could be precipitated in a highly reproducible reaction following the fusion of droplet pairs consisting of different reagents in a hydrodynamically coupled, single-nozzle microfluidic device. Controlled pairwise mixing of aqueous droplets in oil was produced by electrocoalescence [48] and the droplets were prevented from fusing prematurely by using a uniformly distributed surfactant at the interfaces of both droplets. The methodology developed by these researchers could be readily adapted to incorporate the findings of the present manuscript by isolating the surfactant to one of the inlet droplet flows, while leaving the other surfactant-free. Upon merging, Marangoni-induced flows would produce pronounced bulk mixing between the drops, like those explored here. Moreover, enhanced control over the degree of mixing obtained between the drops at different timescales could be explored with the previously discussed surfactant selection criteria.

In this study, we proposed a simple, yet robust experimental methodology for directly quantifying the solutal Marangoni timescales of surface active compounds at the oil-water interface under an induced concentration gradient. With this method, the spreading efficiencies and encouragement of bulk fluid mixing for potentially any surfactant type at the oil water interface can be economically measured. The insights garnered from this work provide a compelling alternative route for inducing bulk flows in microfluidic devices without the need for modulating bulk phase viscosities.

Acknowledgements

Financial support for this work was provided by the National Science Foundation through the East Asia and Pacific Summer Institutes (EAPSI) Fellowship Program (Award Number: 1713936). The authors would also like to thank the anonymous reviewer whose thorough comments and suggestions led to a substantially improved manuscript.

References

[1] J.D. Paulsen, Approach and coalescence of liquid drops in air, Phys. Rev. E – Stat. Nonlinear Soft Matter Phys. 88 (2013) 1–13, https://doi.org/10.1103/PhysRevE.88.063010.
[2] J. Qian, C.K. Law, Regimes of coalescence and separation in droplet collision, J. Fluid Mech. 331 (1997) 59–80.
[3] J.D. Paulsen, R. Carmigniani, A. Kannan, J.C. Burton, S.R. Nagel, Coalescence of bubbles and drops in an outer fluid, Nat. Commun. 5 (2014) 3182, https://doi.org/10.1038/ncomms4182.
[4] J. Eggers, J.R. Lister, H.A. Stone, Coalescence of liquid drops, J. Fluid Mech. (1999) 1–37, https://doi.org/10.1017/S002211209900662X.
[5] L. Duchemin, J. Eggers, C. Josserand, Inviscid coalescence of drops, J. Fluid Mech. 487 (2003) 167–178, https://doi.org/10.1017/S0022112003004646.
[6] D.T. Wasan, The role of coalescence phenomena and interfacial rheological properties in enhanced oil recovery: an overview, J. Rheol. (N. Y. N. Y) 23 (1979) 181, https://doi.org/10.1122/1.549524.
[7] S. Tcholakova, N.D. Denkov, T. Banner, Role of surfactant type and concentration for the mean drop size during emulsification in turbulent flow, Langmuir 20 (2004) 7444–7458, https://doi.org/10.1021/la049335a.
[8] A.M. Huebner, C. Abell, W.T.S. Huck, C.N. Baroud, F. Hollfelder, Monitoring a reaction at submillisecond resolution in picoliter volumes, Anal. Chem. 83 (2011) 1462–1468, https://doi.org/10.1021/ac103234a.
[9] J.H. Kim, T.Y. Jeon, T.M. Choi, T.S. Shim, S.H. Kim, S.M. Yang, Droplet microfluidics for producing functional microparticles, Langmuir 30 (2014) 1473–1488, https://doi.org/10.1021/la403220p.
[10] A.B. Pawar, M. Caggioni, R. Ergun, R.W. Hartel, P.T. Spicer, Arrested coalescence in Pickering emulsions, Soft Matter 7 (2011) 7710, https://doi.org/10.1039/c1sm05457k.
[11] P. Dahiya, M. Caggioni, P.T. Spicer, Arrested coalescence of viscoelastic droplets: polydisperse doublets, Philos. Trans. R. Soc. A Math. Phys Eng. Sci. 374 (2016) 1–13, https://doi.org/10.1098/rsta.2015.0132.
[12] K. Ward, Z.H. Fan, Mixing in microfluidic devices and enhancement methods, J. Micromech. Microeng. 25 (2015) 094001, https://doi.org/10.1088/0960-1317/25/9/094001.
[13] T. Tofteberg, M. Skolimowski, E. Andreassen, O. Geschke, A novel passive micromixer: lamination in a planar channel system, Microfluid. Nanofluidics. 8 (2010) 209–215, https://doi.org/10.1007/s10404-009-0456-z.
[14] T.J. Johnson, D. Ross, L.E. Locascio, Rapid microfluidic mixing, Anal. Chem. 74 (2002) 45–51, https://doi.org/10.1021/ac010895d.
[15] T. Krebs, C.G.P.H. Schroën, R.M. Boom, Coalescence kinetics of oil-in-water emulsions studied with microfluidics, Fuel 106 (2013) 327–334, https://doi.org/10.1016/j.fuel.2012.10.067.
[16] A. Arbor, G. Tryggvason, The Flow Induced by the Coalescence of Two Initially Stationary Drops, Nasa Tech, Memo, 1994.

[17] E. Nowak, N.M. Kovalchuk, Z. Che, M.J.H. Simmons, Effect of surfactant concentration and viscosity of outer phase during the coalescence of a surfactant-laden drop with a surfactant-free drop, Colloids Surf. A Physicochem. Eng. Asp. 505 (2016) 124–131, https://doi.org/10.1016/j.colsurfa.2016.02.016.
[18] E. Nowak, Z. Xie, N.M. Kovalchuk, O.K. Matar, M.J.H. Simmons, Bulk advection and interfacial flows in the binary coalescence of surfactant-laden and surfactant-free drops, Soft Matter 13 (2017) 4616–4628, https://doi.org/10.1039/C7SM00328E.
[19] C.V. Sternling, L.E. Scriven, Interfacial turbulence: hydrodynamic instability and the marangoni effect, AIChE J. 5 (1959) 514–523, https://doi.org/10.1002/aic.690050421.
[20] L.E. Scriven, C.V. Sternling, The Marangoni effects, Nature 187 (1960) 186–188, https://doi.org/10.1038/187186a0.
[21] D.T. Wasan, Destabilization of Water-in-Oil Emulsions, in: Emuls. – A Fundam. Pract. Approach, 1992: pp. 283–295.
[22] M. Saad Bhamla, C. Chai, M.A. Àlvarez-Valenzuela, J. Tajuelo, G.G. Fuller, Interfacial mechanisms for stability of surfactant-laden films, PLoS One 12 (2017) 1–14, https://doi.org/10.1371/journal.pone.0175753.
[23] K. Szymczyk, B. Jańczuk, The adsorption at solution-air interface and volumetric properties of mixtures of cationic and nonionic surfactants, Colloids Surf. A Physicochem. Eng. Asp. 293 (2007) 39–50, https://doi.org/10.1016/j.colsurfa.2006.07.006.
[24] B. Jańczuk, A. Zdziennicka, W. Wójcik, The properties of mixtures of two anionic surfactants in water at the water | air interface, Colloids Surf. A Physicochem. Eng. Asp. 220 (2003) 61–68, https://doi.org/10.1016/S0927-7757(03)00060-8.
[25] S.D. Hudson, A.M. Jamieson, B.E. Burkhart, The effect of surfactant on the efficiency of shear-induced drop coalescence, J. Colloid Interface Sci. 265 (2003) 409–421, https://doi.org/10.1016/S0021-9797(03)00396-5.
[26] W.H. Weheliye, T. Dong, P. Angeli, On the effect of surfactants on drop coalescence at liquid/liquid interfaces, Chem. Eng. Sci. 161 (2017) 215–227, https://doi.org/10.1016/j.ces.2016.12.009.
[27] L. Frenz, A. El Harrak, M. Pauly, S. Bégin-Colin, A.D. Griffiths, J.C. Baret, Droplet-based microreactors for the synthesis of magnetic iron oxide nanoparticles, Angew. Chemie – Int. Ed. 47 (2008) 6817–6820, https://doi.org/10.1002/anie.200801360.
[28] H. Diamant, D. Andelman, Kinetics of surfactant adsorption at fluid-fluid interfaces, J. Phys. Chem. 100 (1996) 13732–13742, https://doi.org/10.1021/jp960377k.
[29] K. Eliceiri, C.A. Schneider, W.S. Rasband, K.W. Eliceiri, NIH Image to ImageJ : 25 years of image analysis, Nat. Methods. 9 (2012) 671–675, https://doi.org/10.1038/nmeth.2089.
[30] D.F. Evans, H. Wennerström, The Colloidal Domain: where Physics, Chemistry, Biology, and Technology Meet, second ed., 1999.
[31] J.J. Nash, K.A. Erk, Stability and interfacial viscoelasticity of oil-water nanoemulsions stabilized by soy lecithin and Tween 20 for the encapsulation of bioactive carvacrol, Colloids Surfaces A Physicochem. Eng. Asp. 517 (2017) 1–11, https://doi.org/10.1016/j.colsurfa.2016.12.056.
[32] J.D. Berry, M.J. Neeson, R.R. Dagastine, D.Y.C. Chan, R.F. Tabor, Measurement of surface and interfacial tension using pendant drop tensiometry, J. Colloid Interface Sci. 454 (2015) 226–237, https://doi.org/10.1016/j.jcis.2015.05.012.
[33] G. Loglio, P. Pandolfini, R. Miller, A.V. Makievski, F. Ravera, M. Ferrari, L. Liggieri, Drop and bubble shape analysis as a tool for dilational rheological studies of interfacial layers, in: D. Möbius, R. Miller (Eds.), Nov. Methods to Study Interfacial Layers, Elsevier, 2001, pp. 439–483. http://doi.org/10.1016/S1383-7303(01)80038-7.
[34] K.H. Kang, H.U. Kim, K.H. Lim, Effect of temperature on critical micelle concentration and thermodynamic potentials of micellization of anionic ammonium dodecyl sulfate and cationic octadecyl trimethyl ammonium chloride, Colloids Surfaces A Physicochem. Eng. Asp. 189 (2001) 113–121, https://doi.org/10.1016/S0927-7757(01)00577-5.
[35] V. Mosquera, J.M. Del Río, D. Attwood, M. García, M.N. Jones, G. Prieto, M.J. Suarez, F. Sarmiento, A study of the aggregation behavior of hexyltrimethylammonium bromide in aqueous solution, J. Colloid Interface Sci. 206 (1998) 66–76, https://doi.org/10.1006/jcis.1998.5708.
[36] T.G. Movchan, A.I. Rusanov, I.V. Soboleva, N.R. Khlebunova, E.V. Plotnikova, A. K. Shchekin, Diffusion Coefficients of Ionic Surfactants, Colloid J. 77 (2015) 492–499, https://doi.org/10.1134/S1061933X15040146.
[37] M.J. Rosen, Surfactants and Interfacial Phenomena, third ed., John Wiley & Sons Inc, 2004.
[38] J. Eastoe, S. Nave, A. Downer, A. Paul, A. Rankin, J. Penfold, Adsorption of ionic surfactants at the air – solution interface, Langmuir 16 (2000) 4511–4518, https://doi.org/10.1021/la991564n.
[39] B.J. Park, J. Pantina, E.M. Furst, M. Oettel, S. Reynaert, Direct measurements of the effects of salt and surfactant on interaction forces between colloidal particles at water-oil interfaces, Langmuir 24 (2008) 1686–1694, https://doi.org/10.1021/la7008804.
[40] B.P. Binks, Particles as surfactants – similarities and differences, Curr. Opin. Colloid Interface Sci. 7 (2002) 21–41, https://doi.org/10.1016/S1359-0294(02)00008-0.
[41] M. Wu, T. Cubaud, C. Ho, Scaling law in liquid drop coalescence driven by surface tension, Phys. Fluids 16 (2004) 51–54, https://doi.org/10.1063/1.1756928.
[42] S.J. Rehfeld, Adsorption of sodium dodecyl sulfate at variuous hydrocarbon-water interfaces, J. Phys. Chem. 71 (1967) 738–745, https://doi.org/10.1021/j100862a039.
[43] V.B. Fainerman, E.V. Aksenenko, N. Mucic, A. Javadi, R. Miller, Thermodynamics of adsorption of ionic surfactants at water/alkane interfaces, Soft Matter 10 (2014) 6873–6887, https://doi.org/10.1039/C4SM00463A.
[44] A. Prins, C. Arcuri, M. Van den Tempel, Elasticity of thin liquid films, J. Colloid Interface Sci. 24 (1967) 84–90, https://doi.org/10.1016/0021-9797(67)90281-0.
[45] A. Javadi, N. Mucic, D. Vollhardt, V.B. Fainerman, R. Miller, Effects of dodecanol on the adsorption kinetics of SDS at the water–hexane interface, J. Colloid Interface Sci. 351 (2010) 537–541, https://doi.org/10.1016/j.jcis.2010.07.033.
[46] C. Stubenrauch, V.B. Fainerman, E.V. Aksenenko, R. Miller, Adsorption behavior and dilational rheology of the cationic alkyl trimethylammonium bromides at the water/air interface, J. Phys. Chem. B 109 (2005) 1505–1509, https://doi.org/10.1021/jp0465251.
[47] V. Seredyuk, E. Alami, M. Nydén, K. Holmberg, A.V. Peresypkin, F.M. Menger, Adsorption of zwitterionic gemini surfactants at the air-water and solid-water interfaces, Colloids Surf. A Physicochem. Eng. Asp. 203 (2002) 245–258, https://doi.org/10.1016/S0927-7757(01)01106-2.
[48] K. Ahn, J. Agresti, H. Chong, M. Marquez, D.A. Weitz, Electrocoalescence of drops synchronized by size-dependent flow in microfluidic channels, Appl. Phys. Lett. 88 (2006), https://doi.org/10.1063/1.2218058.